Pamukkale Univ Muh Bilim Derg, 30(4), 451-462, 2024

Pamukkale Üniversitesi Mühendislik Bilimleri Dergisi

Pamukkale University Journal of Engineering Sciences

Electrical sizing of grid-connected photovoltaic systems

Şebekeye bağlı fotovoltaik sistemlerin elektriksel boyutlandırılması

Ahmet ILICA[1*], *Muhammed SERDAR*[2]

[1]Department of Electricity and Energy, Simav Vocational School, Kütahya Dumlupınar University, Kütahya, Turkey.
ahmet.ilica@dpu.edu.tr

[2]SMS Energy Consulting R&D Engineering Limited Company, Denizli, Turkey.
m.serdar@smsenerji.com

Received/Geliş Tarihi: 07.11.2022 Revision/Düzeltme Tarihi: 02.06.2023 doi: 10.5505/pajes.2023.24896
Accepted/Kabul Tarihi: 14.08.2023 Research Article/Araştırma Makalesi

Abstract

It is of great importance to choose low-cost, high-performance/efficient and operating and protection equipment in accordance with the applicable legislation in electrical facilities. It is necessary to make calculations for the selection of the most suitable cable/line, measuring and protection system equipment. In this study, panel-inverter compatibility calculation, voltage drop, current control, short circuit, lightning risk and protection calculations, grounding resistance and grounding conductor calculations and tilt angle calculation were made for a grid connected photovoltaic system with a power of 0.4 MWe. It has been calculated that the allowable voltage range and maximum powerpoint voltage values of the selected inverter are compatible with the panel system. With voltage drop and current control calculations, copper cable cross section for each inverter output and solar board output were found to be 3x70+35 mm² and 2(3x185+95) mm², respectively, and transformer low voltage busbar 60x10 mm². In order not to deform the low voltage busbars in peak short-circuit current, they should be placed at 10 cm intervals for 80 cm length. According to the transformer low voltage side phase-earth short circuit current, the cross-section of the grounding conductor should be at least 53.97 mm² copper conductor. In the lightning protection facility of the panels, according to the rolling sphere method, it has been calculated that the air termination rods should be at least 0.84 m above the upper point of the solar panel. The optimum fixed panel tilt angle was found to be 32.08°. The calculations used in the study will benefit the practitioners in the design of grid-connected photovoltaic systems, in the selection of the most suitable electrical equipment with minimum size.

Keywords: Grid connected photovoltaic system, Voltage drop, Short circuit calculation, Lightning protection, Tilt angle.

Öz

Elektrik tesislerinde düşük maliyetli, yüksek performanslı/verimli ve ilgili mevzuata uygun işletme ve koruma ekipmanlarının seçilmesi büyük önem taşımaktadır. En uygun kablo/hat, ölçüm ve koruma sistemi ekipmanlarının seçimi için hesaplamalar yapılması gerekmektedir. Bu çalışmada, şebeke bağlantılı 0.4 MWe gücünde bir fotovoltaik sistem için panel-evirici uyumluluk hesabı, gerilim düşümü, akım kontrolü, kısa devre, yıldırım risk ve koruma hesapları, topraklama direnci ve topraklama iletkeni hesapları ve panel eğim açısı hesabı yapılmıştır. Seçilen eviricinin izin verilen voltaj aralığı ve maksimum güç noktası gerilim değerlerinin panel sistemi ile uyumlu olduğu hesaplanmıştır. Gerilim düşümü ve akım kontrol hesapları ile her evirici çıkışı ve güneş sistemi panosu çıkışı için bakır kablo kesiti sırasıyla 3x70+35 mm² ve 2(3x185+95) mm², trafo alçak gerilim barası 60x10 mm² olarak bulunmuştur. Alçak gerilim baralarının tepe kısa devre akımında deforme olmaması için 80 cm boy için 10 cm aralıklarla yerleştirilmelidir. Trafo alçak gerilim tarafı faz-toprak kısa devre akımına göre topraklama iletkeninin kesiti en az 53.97 mm² bakır iletken olmalıdır. Panellerin yıldırımdan korunma tesisinde yuvarlanan küre yöntemine göre, hava yakalama uçlarının güneş panelinin üst noktasından en az 0.84 m yukarıda olması gerektiği hesaplanmıştır. Optimum sabit panel eğim açısı 32.08° bulunmuştur. Çalışmada kullanılan hesaplamalar, şebeke bağlantılı fotovoltaik sistemlerin tasarımında, minimum boyutta en uygun elektriksel donanımın seçiminde uygulayıcılara fayda sağlayacaktır.

Anahtar kelimeler: Şebekeye bağlı fotovoltaik sistem, Gerilim düşümü, Kısa devre hesabı, Yıldırımdan koruma, Eğim açısı.

1 Introduction

The possibility of depletion of fossil fuels, the environmental effects they cause, the increase in the use of energy-related technology, the decrease in system costs and the economic support provided by the tariff guarantee have made the use of photovoltaic (PV) systems widespread. Renewable energy-based production reduces environmental problems such as air pollution, climate change and global warming caused by fossil fuels [1]. PV energy is clean, quiet, abundant, sustainable, modular, long-lasting and renewable as well as reliable. The use of PV systems for electricity generation prevents environmental pollution caused by carbon emissions, oil spills and toxic by-products caused by fossil fuels. A 1 kW PV system that generates 150 kWh of energy every month prevents the extraction of 75 kg of fossil fuel, the emission of 150 kg of CO2 into the atmosphere and the consumption of 473 L of water [2],[3]. With the developing technology, the costs of PV systems are decreasing and accordingly their use is becoming widespread [4],[5]. PV systems are basically applied in two different ways, off-grid and grid-connected. Grid-connected PV systems consist of two types. In the first type, the generated energy is fed directly to the grid. In the second, after the internal need is met, the excess energy is given to the grid and energy is taken from the grid when necessary [6]. Grid-connected systems have advantages such as the possibility of being consumed in loads close to where the energy is produced, and the absence of battery costs and losses. In addition, surplus generation can be given to the grid, and loads can be fed from the grid in case of production deficiency and failure. Losses from cables, inverter and panel-inverter incompatibility occur in well-designed PV systems where there is no shading [7]. It is

*Corresponding author/Yazışılan Yazar

desired to be able to work at the maximum powerpoint in the systems connected to the grid, to transfer controlled power to the grid, low harmonic distortion and high power factor. In order to prevent islanding during grid outages, the system should be separated from the grid with an inverter or additional equipment. Maximum powerpoint tracking (MPPT), which enables the production of maximum power from the light falling on the panel, is provided by DC-DC converters or inverters [8],[9]. The inverters, which are the center of the system, play an important role in energy efficiency and reliability thanks to their MPPT systems [10].

In a PV system, voltage drop and power loss occur in DC and AC sections due to cable internal resistances and length. Increasing the cable length and decreasing its cross-section cause an increase in voltage drop and power loss. Since approximately 6% of the total losses, which constitute 18% of the current energy, occur in the cables, the selection of the section is of great importance in order to reduce these losses. If the cable cross-section is less than the required value, it causes voltage drop and power loss in the conductor, while its large size increases the cost of the system. For this reason, it is necessary to calculate the voltage drop and current control in order to compare the cable sections used in the entire system with critical values in order to meet the safety conditions and to test their compliance with national and international standards. With these calculations, the cable cross-section is selected, the voltage drop of which is less than the critical value and has the capacity to carry the passing current [7],[11],[12].

In electrical installations, parts with different voltages come into contact with each other and cause a short circuit due to reasons such as rupture, displacement, insulation failure. High-value currents resulting from a short circuit not only damage the system, but also pose a life safety hazard. Since short-circuit faults, which have effects such as instability, thermal and mechanical stress in electrical power systems, are removed from the system by the breakers, short-circuit calculations must be made to determine the short-circuit breaking capacities of the breakers [13]. In grid-connected PV systems, short-circuit current is important for the selection of operating equipment and protection setting in thermal magnetic breakers. Asymmetric short circuit failures such as phase-to-phase, two-phase ground, phase-ground occur in power systems in addition to symmetrical failures such as three-phase short circuit where the highest short circuit currents pass [13]. The temperature caused by thermal stress on the cables can cause damage to the cables. For this reason, in addition to current control and voltage drop calculation, cross-section control should be performed according to thermal short-circuit current when determining cable cross-sections.

Grounding is the most effective method in providing life and equipment safety from operating voltage and lightning discharges in PV systems. A facility-wide grounding system is required to ensure that the system complies with safety regulation. The grounding system should ensure that fault currents are transmitted to the ground in the event of a fault, without posing a life safety risk, without exceeding the equipment limits and without adversely affecting the continuity of the service. In grid-connected PV systems, the grounding network should cover the PV system and the substation [14],[15]. External lightning systems are required to protect all components of the PV system from a direct lightning strike, and surge arresters are required to protect DC cables and inverter cables from lightning effects [16]. Rooftop PV systems are vulnerable to direct lightning effects due to their location. In addition to long-term failure of important components such as a possible lightning panel, inverter, it poses a life-threatening danger to people [17]. In order to protect these structures from a direct lightning strike, protection zones should be established and lightning protection systems that transmit the lightning current to the ground in a safe and controlled manner should be installed. In order to protect PV systems from lightning strikes a air termination rod, a landing conductor and electrodes that transmit lightning currents to the ground is installed in the facility. The installation of an efficient lightning protection system for large-scale PV systems prevents the occurrence of any physical damage and life hazards. The cost of installing lightning protection at these facilities is insignificant compared to the loss of income from malfunctions or damage caused by a lightning strike [18],[19].

Selecting larger unit sizes for PV systems causes unnecessary cost increases, while choosing small unit sizes creates failure, overload, damage and safety risks. Therefore, in this study, electrical calculations were made for the selection of operation and protection equipment in cases such as normal operation, short circuit, lightning strike for monocrystalline panel, string inverter PV system with an installed power of 541 kWp DC, 400 kWe AC.

2 Grid-connected PV system structure

The grid-connected photovoltaic system, electrically dimensioned in this study, basically consists of solar panel arrays, carrier system, solar cables, inverters, AC cables and lightning protection system. Grid connection in the system is provided by a transformer station. The general structure of the grid-connected PV system is shown in Figure 1.

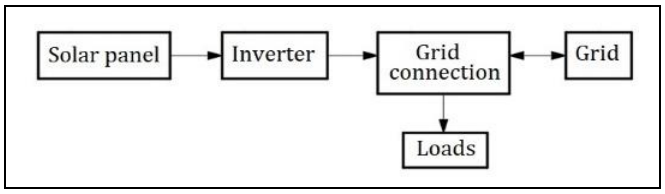

Figure 1. Grid connected PV system block diagram.

Grid-connected photovoltaic systems also include protection and switching equipment, bidirectional meters, energy analyzers, and remote access communication systems. The DC energy produced by the solar panels comes to the inverter via solar cables. AC power from the inverter output directly feeds the load or is connected to the grid with a bidirectional meter and transformer. When the PV system is insufficient, the plant is fed from the grid via transformer and bidirectional meter. The energy flow in both directions on the bidirectional meter is periodically monitored and offset is made with the distribution company.

2.1 Panel-inverter compatibility calculation

Maximum panel power (W_p), maximum power point voltage (V_{MPPT}), open circuit voltage (Voc), short circuit current (I_{sc}) and open circuit voltage temperature coefficient (K_{Voc}) are the important parameters available from the datasheet [20]. The PV module with an efficiency of 20.17% discussed in this study (AE Solar AEHM6-72 370-400W monokristal) parameters for standard test conditions (STC) are shown in Table 1.

Table 1. PV panel values.

W_p (W)	V_{MPPT} (V)	Voc (V)	I_{MPPT}(A)	I_{sc} (A)	Tmax (°C)	Tmin (°C)	K_{Voc} (%/°C)
400	41,71	49,69	9,59	10,59	70	-11,4	-0,28

The STC of PV specifies a PV module with a temperature of 25 °C, an air mass spectrum of 1.5 and a radiation of 1000 W/m² at zero wind speed [21]. The maximum (Tmax) and minimum temperature (Tmin) values in the table are values that vary according to the region where the panel is used. in this study, Denizli province in Turkey is based. This province has a very good solar energy potential with its total solar radiation values of 1550-1750 kWh/m²-year [22]. PV arrays rarely produce the STC rated output voltage due to factors such as meteorological conditions, intermittent character of the radiation and orientation.

Due to the PV/inverter cost ratio and higher inverter efficiency at full loads, it is recommended that the optimum inverter power be smaller than the nominal size of the PV array in the design and installation of grid-tied PV systems [23],[24]. An increase of the inverter power from 80% to 100% provide a 20% increase in the inverter sizing, while the energy increase is at most 2%, so the inverter power can be sized as 65%-80% of the PV array power [1],[24]-[28]. Therefore, in this study, the panel/inverter ratio has been accepted as 1.35. An inverter (SUN2000-100KTL-M1) with AC output power of 100kWe and maximum efficiency 98.8% is based. It is suitable for rooftop and field type grid connected PV systems. The inverters convert the DC voltage generated by the panel arrays into AC voltage compatible with the grid. Four inverters should be used in the system. Inverter values are given in Table 2. Parameters and abbreviations in the table are as follows. The maximum and minimum allowable input voltages (Vin_{max}, Vin_{min}), maximum and minimum MPPT voltages ($V_{MPPTine-max}$, $V_{MPPTine-min}$), maximum current and short-circuit current (Ip_{max}, Ip_{scmax}), the MPPT number for each inverter (n_{MPPT}).

At the same radiation value, the panel produces a higher voltage than the STC when the temperature is low, and a lower voltage when the temperature is high. For this reason, considering the maximum and minimum temperature values in the region where the panel is used, the maximum and minimum number of serial panels suitable for the inverter inputs should be determined by panel-inverter compatibility calculation. In the panel-inverter compatibility calculation, the maximum and minimum open circuit voltages (Voc_{max}, Voc_{min}), maximum and minimum MPPT voltages ($Voc_{max-MPPT}$, $Voc_{min-MPPT}$) that can be taken from a panel are calculated according to the minimum and maximum temperature conditions of the region where the panel is used, by Equation 1-4.

$$Voc_{max} = Voc\left[1 + \left(K_{Voc}.\left(\frac{Tmin - Ts}{100}\right)\right)\right] \quad (1)$$

$$Voc_{min} = Voc\left[1 + \left(K_{Voc}.\left(\frac{Tmax - Ts}{100}\right)\right)\right] \quad (2)$$

$$Voc_{max-MPPT} = V_{MPPT}\left[1 + \left(K_{Voc}.\left(\frac{Tmin - Ts}{100}\right)\right)\right] \quad (3)$$

$$Voc_{min-MPPT} = V_{MPPT}\left[1 + \left(K_{Voc}.\left(\frac{Tmax - Ts}{100}\right)\right)\right] \quad (4)$$

Maximum and minimum panel numbers (N_1, N_2) are found by Equations 5 and 6, respectively, according to the allowed input voltage value range of the inverter. Based on the calculated maximum number of panels, the maximum open circuit voltage ($Voc_{max-string}$), minimum open circuit voltage ($Voc_{min-string}$), maximum MPPT voltage ($V_{MPPTmax-str}$) and minimum MPPT voltage ($V_{MPPTmin-str}$) for an string are calculated by Equation 7-10, respectively.

$$N_1 = \frac{Vin_{max}}{Voc_{max}} \quad (5)$$

$$N_2 = \frac{Vin_{min}}{Voc_{min}} \quad (6)$$

$$Voc_{max-string} = N_1 Voc\left[1 + \left(K_{Voc}.\left(\frac{Tmin - Ts}{100}\right)\right)\right] \quad (7)$$

$$Voc_{min-string} = N_1 Voc\left[1 + \left(K_{Voc}.\left(\frac{Tmax - Ts}{100}\right)\right)\right] \quad (8)$$

$$V_{MPPTmax-str} = N_1 V_{MPPT}\left[1 + \left(K_{Voc}.\left(\frac{Tmin - Ts}{100}\right)\right)\right] \quad (9)$$

$$V_{MPPTmin-str} = N_1 V_{MPPT}\left[1 + \left(K_{Voc}.\left(\frac{Tmax - Ts}{100}\right)\right)\right] \quad (10)$$

The results from Equation 7-10 are compared with the inverter values. The string open circuit and MPPT voltage values must be within the inverter value range.

2.2 Current control and voltage drop calculation

In this study, the voltage drop calculation in the grid connected PV system has been made for the plant sections numbered among the components in the block diagram in Figure 2. The dashed section shows the monoblock concrete kiosk (MCK) and second transformer substation (TS 2).

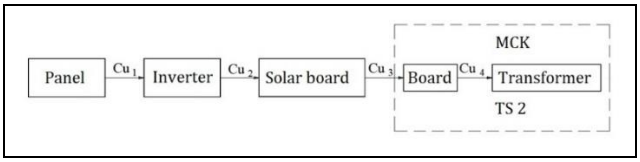

Figure 2. PV system wiring structure block diagram.

AC cable current (I), corrected current (Id_{AC}), percent voltage drop (e%), DC panel cable corrected current (Id_{DC}), percent power loss (p_L%), respectively calculated by Equation 11-16.

$$I = \frac{S}{\sqrt{3} \times U_{AC}} \quad (11)$$

$$Id_{AC} = I\, k_1\, k_2 \quad (12)$$

$$e_{AC}\% = \frac{100\, L\, P}{k\, s\, U_{AC}^2} \quad (13)$$

Table 2. Inverter values.

Vin_{max}(V)	Vin_{min}(V)	$V_{MPPTin-max}$(V)	$V_{MPPTin-min}$(V)	Ip_{scmax}(A)	Ip_{max}(A)	n_{MPPT}
1000	200	1000	200	40	26	10

$$Id_{DC} = \frac{I_P}{k_1\, k_2} \tag{14}$$

$$e_{DC}\% = \frac{200\, L\, P}{k\, s\, U_{DC}^2} \tag{15}$$

$$p_L\% = \frac{300\, I_p^2\, L}{k\, s\, P} \tag{16}$$

Where S, apparent power U_{AC}, inverter output line voltage k_1, cable temperature coefficient k_2, cable carry correction coefficient R, cable resistance L, cable length P, active power k, conductivity coefficient (56 m/Ωmm² for copper conductor) s, cable cross section I_P, is the panel current and U_{DC} is the string DC voltage.

2.3 Short circuit calculation

Symmetrical/sequence components method is used to calculate the currents caused by balanced and unbalanced short circuits in three-phase systems. In this method, the current in each line is found by summing the currents belonging to the system with three symmetrical components [13]. The symmetric components method, which uses zero sequence component (ZS), correct component or positive sequence component (PS) and inverse component or negative sequence component (NS) in short circuit failures, facilitates the analysis of the system. ZS, PS, and NS are denoted by the indices 0, 1, and 2, respectively. Industry standard IEC 60909 is widely used when performing short-circuit studies in conventional and renewable energy systems, giving results with acceptable accuracy [29]. In this study, short circuit calculations were made with per-unit (pu) values. Since the calculation of the impedances as pu values according to the selected base power ensures that they are independent of voltage, the short-circuit calculation with the pu method provides convenience and practicality compared to the calculation made according to the physical values [30]. The grid connection structure of the PV system is shown in Figure 3.

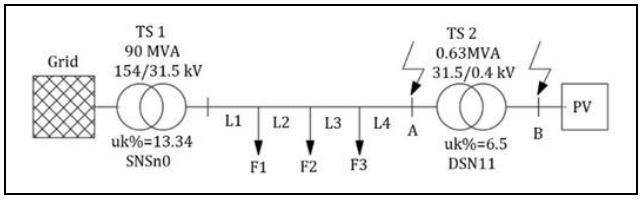

Figure 3. PV system grid connection structure.

The mains connection is provided by the line divided by the medium voltage consumer lines F1, F2 and F3. The load connected to point B in the system is fed, and the excess energy is sent to the grid. When the power requirement cannot be provided by the PV system, energy is taken from the grid. In the system, short-circuit analysis of points A and B was carried out using the impedance values of the network, 90 MVA first transformer substation (TS 1), L1, L2, L3, L4 lines and 0.63 MVA TS 2.

In the L1, L2, and L3 line sections, 3 pieces of 80 m long (1x95) mm² copper XLPE, 500 m long 3/0 AWG Piegon, and 1200 m long 3/0 AWG are used, respectively. For the 30 m long L4, aluminum XLPE cable is taken as the basis and its cross-section will be determined in this study according to the thermal short circuit current. The NYY cable to be used at the B bus output (shown as Cu_4 in Figure 2) and the copper bus section are determined according to current control, voltage drop and thermal short circuit current. In low voltage copper busbars, bending stress is calculated for the appropriate busbar length and distance between the busbars. While calculating the short circuit, the system voltage is taken as the base voltage in the system and the base power (S_b) is taken as 100 MVA. The short-circuit power of the system ($S_k^{"}$), given the initial three-phase short-circuit current ($I_{k3}^{"}$) in the power network (grid), is calculated by Equation 17.

$$S_k^{"} = \sqrt{3}\; I_{k3}^{"}\, U_n \tag{17}$$

U_n is the rated voltage. When calculating the short-circuit currents, the transition resistances are assumed to be zero and the continuous operating currents are neglected. The pu sequence components used for the resistance and reactances of the power transmission system, transformers and lines in short circuit calculations are given in the Equations below. The positive and negative sequence components are considered equal in the whole system [30],[31]. In the power system (grid), the reactance of the positive order component (X_{1Spu}) and the zero order component (X_{0Spu}) pu is calculated by Equations 18 and 19.

$$X_{1Spu} = \frac{S_b}{S_k^{"}} \tag{18}$$

$$X_{0Spu} = 2\, X_{1Spu} \tag{19}$$

The zero sequence component resistance is taken equal to the positive sequence component, while the positive sequence component pu resistance (R_{1Spu}) can be found by Equation 20, [13],[31].

$$R_{1Spu} = 0.1\, X_{1Spu} \tag{20}$$

The positive sequence component real (X_{1TR}) and pu reactances (X_{1TRpu}) in transformers are found by Equations 21 and 22, respectively. The zero order component is equal to the positive order component [30].

$$X_{1TR} = u_k\% \frac{U_{nTR}}{S_{nTR}} \tag{21}$$

$$X_{1TRpu} = \frac{u_k}{S_{tr}} \tag{22}$$

The ohmic resistance sequence components in the transformer are zero. In the star-point grounding resistance of the star-to-star connected transformer in TS 1, while the sequence component reactances and the positive sequence component ohmic resistance are zero, the zero sequence

component ohmic resistance (R_{0npu}) is found according to Equation 23. R_N is the resistance between star point TS 1 and ground. Equation 24 is used to calculate the positive sequence component pu reactances (X_{1Lpu}) in all cables and lines [30].

$$R_{0npu} = \frac{3\ R_N\ S_b}{Un^2} \tag{23}$$

$$X_{1Lpu} = \frac{x\ l\ S_b}{U_n^2} \tag{24}$$

Here, x is the reactance of one kilometer of cable and l is the length of the cable. The zero sequence component reactance depends on the environment of the cable. Cable sheath and cable construction are important as zero currents are determined by the ground, metal structures, cable shield, cable sheaths [30]. In steel aluminum overhead lines and underground cables zero sequence component reactances (Xh_{0Lpu}, Xy_{0Lpu}) can be calculated as Equations 25 and 26, respectively, by finding the tables prepared according to the zero current circuit completion path. These values vary according to cable type and placement [30].

$$Xh_{0Lpu} = 2.9\ X_{1Lpu} \tag{25}$$

$$Xy_{0Lpu} = 7\ X_{1Lpu} \tag{26}$$

The positive sequence component for the pu resistor (R_{1L}) in cables and lines is found as in Equation 27. r is the resistance of one kilometer cable.

$$R_{1L} = \frac{r\ l\ S_b}{U_n^2} \tag{27}$$

The pu resistance (Rh_{0Lpu}) is found with Equation 28 by adding 0.15 Ω/km to the ohmic resistance for the return resistance of the short-circuit current from the ground in the zero sequence component overhead lines. For underground cables, pu resistance (Ry_{0Lpu}) can be calculated with Equation 29 using the tables prepared according to core cross-section and operating voltage [30], [31].

$$Rh_{0Lpu} = \frac{(r + 0.15)l\ S_b}{Un^2} \tag{28}$$

$$Ry_{0Lpu} = 3\ R_{1L} \tag{29}$$

The impedance value (Z_{pu}) is found by using the resistance and reactance pu values calculated according to the selected base power. The maximum base current (I_b) according to the base power and base voltage is calculated by Equation 30.

$$I_b = \frac{S_b}{\sqrt{3}\ U_b} \tag{30}$$

Three-phase short-circuit pu current (Ik''_{3pu}) is calculated according to Equation 31 by using the equivalent of the base voltage value as the unit value at the selected base power.

$$Ik''_{3pu} = \frac{U_{pu}}{Z_{pu}} \tag{31}$$

Short-circuit currents are calculated after the resistance and reactance pu values for the whole system are found. In short-circuit calculations, the initial value of the short-circuit current is shown as Ik'', the continuous short-circuit current Ik, and the instantaneous short-circuit apparent power Sk''. Three phase short circuit current (Ik''_3), two phase short circuit current (Ik_2''), phase ground short circuit current (Ik_{1t}''), two phase ground short circuit current (Ik_{2t}'') for points A and B of the system are calculated by Equations 32-35, respectively [30].

$$Ik''_3 = Ik''_{3pu}\ I_b \tag{32}$$

$$Ik_2'' = \left(\frac{\sqrt{3}}{2}\right)\ Ik''_3 \tag{33}$$

$$Ik_{1t}'' = Ik_3''\ \left(\frac{3}{(2+k)}\right) \tag{34}$$

$$Ik_{2t}'' = Ik_3''\ \left(\frac{3}{(1+2k)}\right) \tag{35}$$

Here, k is the ratio of zero sequence impedance component/positive sequence impedance component at the short-circuit point. In case of a short circuit, a force occurs between the poorly fixed conductors and this force may cause damage to the conductor [31]. For this reason, peak short-circuit current calculation is made to ensure that the equipment to be selected can withstand the dynamic effect of short-circuit currents. The pulse/peak short-circuit current corresponding to the maximum (peak) value of the short-circuit current is found according to the maximum calculated fault current value. Peak short-circuit current (I_p) is calculated by Equation 36.

$$I_p = \kappa\sqrt{2}\ Ik''_{maks} \tag{36}$$

Where Ik''_{maks} is the largest short-circuit current in the busbar, and κ is the peak short-circuit current coefficient. κ is calculated approximately from the R/X ratio graphs or by Equation 37.

$$\kappa = 1.02 + 0.98e^{-3R/X} \tag{37}$$

Peak short-circuit current is used in the selection and sizing of breaker, current transformer and busbar conductor [30].

Cables used in electrical installations should be examined in terms of voltage drop and current carrying capacity as well as short circuit [13]. Short circuit fault causes thermal and dynamic stress of cables and busbars. The thermal stress depends on the magnitude and duration of the short-circuit current. Therefore, the thermal short-circuit current (I_{th}) has to be calculated using Equation 38.

$$I_{th} = Ik''_{maks}\ \sqrt{(\ (m + n)t\ )} \tag{38}$$

In the given expression t is the time to clear the fault and is usually taken as 0.5 s.

In the thermal short-circuit current Equation, m value, which is the heat effect value produced by the direct current component of the short-circuit current, is found from the average thermal short-circuit currents curve according to t and κ or from Equation 39 [13],[30]. f is the rated frequency.

$$m = \frac{(e^{4\ f.t.\ln(\kappa-1)} - 1)}{2\ f\ t\ \ln(\kappa - 1)} \tag{39}$$

The value of n in Equation 38 is the heat effect produced by the alternating current component of the short-circuit current. The short-circuit current shape changes depending on

whether the fault is close or far from the source. Short circuits with a time-invariant current characteristic where the initial short-circuit current is equal to the continuous short-circuit current are short-circuits far from the source. Short circuits in which the initial short-circuit current portion is high and the continuous state is small are defined as short-circuits close to the source [31]. In short circuits where the fault location is far from the source, the initial symmetrical short-circuit current is equal to the steady-state short-circuit current. The value in the thermal short circuit expression is found from the thermal short circuit currents curve according to the value of Ik''/Ik and t. [30],[31]. Since short-circuit currents are high especially in production centers, transformer stations and nearby, the resistance of cables against short-circuit currents should be calculated. The section suitability calculation according to the thermal short-circuit current is made by Equation 40.

$$q_{th} = \frac{I_{th}}{j_{th}} \tag{40}$$

Where I_{th} is the thermal short circuit current, j_{th} is the current density of the conductor used. Current density According to the conductor temperature at the beginning of the short circuit and the duration of 1sec, the minimum current density is 115 A/mm² for copper conductors, 120 A/mm² for copper busbars, 94 A/mm² for aluminum XLPE conductors can be used [30]-[32]. Since the thermal short-circuit current is especially important in terms of the thermal resistance of current transformers [30]. Value of current transformers according to thermal short circuit current is calculated by Equation 41.

$$I_{thCT} = \frac{I_{th}}{I_{CT}} I_n \tag{41}$$

Here, the maximum thermal short circuit current passing through the line to which the I_{th} current transformer is connected is the current value passing through the primary of the I_{CT} current transformer.

The circuit breakers must be capable of breaking the current that may occur in case of a full short circuit in the facility [33]. When selecting the circuit breaker, the selection is made according to the largest short-circuit current. When the breaking time is 100 ms, the maximum short-circuit current breaking current coefficient is multiplied by 1.1 and Ia is obtained. The short-circuit breaking apparent power (Sa"), which is the most important factor in breaker selection, is found by Equation 42, [34].

$$Sa'' = \sqrt{3}\, Un\, Ia \tag{42}$$

In the selection of transformer low voltage side breaker, the highest short-circuit current is 25% more than the calculated maximum short-circuit current. The dynamic withstand current of the current transformers is calculated by taking the rated current 2.5 times more than the thermal withstand current [34].

Current carrying capacity, thermal short-circuit current and peak short-circuit current are based on the selection of the TS 2 low voltage side busbar in the grid-connected PV system. Choosing the right busbar is important for the operation and safe use of the system. In order to determine the bending stress of the busbar, the stress generated by the peak force caused by the peak short-circuit current must be calculated [35]. The bending stress applied to the busbar must not exceed a certain value. When it is assumed that the system consists of three phases, one busbar for each phase, the busbar current intensity is the same and the busbars are placed vertically, the bending stress caused by the electrodynamic force between the busbars is calculated by Equation 43.

$$\sigma_g = v_\sigma \beta \frac{3\, \mu_0 k_D I_p^2 l^2}{8\, \pi\, a\, h\, b^2} \leq \sigma_{dop} \tag{43}$$

Where, μ_0 magnetic field constant ($4\pi 10^{-7}$ H/m), k_D Dwing coefficient (1 can be taken), I_p peak short-circuit current, l busbar length, a is distance between bars, h busbar length, b busbar width, v_σ bending stress factor (1 can be taken), β is the support factor (1 for the insulator supported system), σ_{dop} is the bending stress values allowed in the standards [36].

2.4 Lightning protection and grounding system calculation

For lightning protection application, it is necessary to calculate the lightning risk by taking into account the losses that may occur in case of damage. Lightning risk calculation can be made according to IEC or NFC 17-102 standards. When calculating the risk, the frequency of direct lightning strikes on the structure in a year, the probability of damage that may occur, the amount of material loss that may occur as a result of damage are taken into account [37]. In this method, the length, width and height dimensions of the area to be protected are taken into account. In the method that gives better results in rectangular areas, the equivalent area of the protection zone (A_e) is found by Equation 44 in the calculation made according to the effective equivalent area method [37]-[40].

$$A_e = LW + 6H(L + W) + 9\pi H^2 \tag{44}$$

Here, L is the plant length, W is the plant width, and H is the plant height. Lightning intensity calculation (N_g) according to the number of lightning days in the area to be protected is done with Equation 45.

$$N_g = 0.04\, T_d^{1,25} \tag{45}$$

T_d is the expected number of stormy days per year for the facility and is looked at from the isochronic map (Td=11.9 in this study). The expected lightning number for the facility (N_d) is found by Equation 46.

$$N_d = N_g\, A_e\, C_1\, 10^{-6} \tag{46}$$

C_1 value varies depending on whether the building is the tallest building in the region or whether it is surrounded by higher trees or buildings [40]. In the PV system, the coefficient is determined based on the height of the facility relative to the surrounding structures. The number of lightning strikes approved for the facility or the acceptable number of lightning strikes to the facility is calculated by Equation 47.

$$N_c = 5.5\, 10^{\left(\frac{-3}{C_2 C_3 C_4 C_5}\right)} \tag{47}$$

While C_2 is a coefficient related to the building and roof building material, C_3 is a coefficient of structural value, C_4 is a coefficient related to the occupancy of the building, and C_5 is a coefficient related to environmental importance. After the lightning risk calculation is made for the PV system, it must be protected by the appropriate lightning protection method.

Generally, isolated or non-isolated lightning protection systems are preferred to the panel using Franklin rods. In isolated systems, the air-termination rods are positioned away from the panel, while in non-isolated systems, the air-termination rod is part of the panel support assembly [41]. In high-risk damage situations, the isolated system is widely used. The primary goal of designing a lightning protection and grounding system for a large-scale PV application is to strike a balance between the cost of installation and the efficiency and life of the system [19]. The main design methods of air-termination rod based systems are the protection angle or rolling sphere method formed by the network structure. The protection angle method assumes that there are a number of air termination rods installed along the entire length of the PV support infrastructure, which have a sufficient height and provide the required protection angle. In the rolling sphere method, the air termination rods are positioned to prevent all parts of the panel and supporting substructure from coming into contact with a sphere of radius R. A protective conductor is installed at the contact points of the sphere to the structure. Sphere center represents the geometric location of the points where lightning discharge may ocur [18]. In this study, the rolling sphere method is used to protect the PV system from lightning. In the rolling sphere method, four levels of classification are made for lightning protection. Level I is the most sensitive and the rolling sphere radius is taken as 20m, while IV is the coarsest protection level and the sphere radius is taken as 60m. In the rolling sphere method, the sphere, which acts like a conductive lightning ball, has the risk of striking the points it contacts while rolling all over the structure, so these areas must be protected with a air termination rod. The rolling of the sphere in all directions in the structure must be taken into account so that no unprotected surface is left. In the rolling sphere method, the principle structure of which is shown in Figure 4, it is the volume protection zone where the radius of the sphere cannot reach and the rolling sphere cannot enter between the two air termination rod [38],[42],[43].

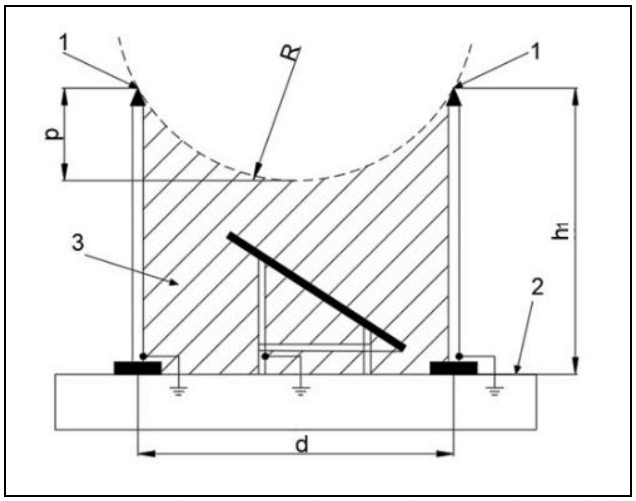

1: Air termination rod. 2: Reference plane, ground. 3: Protected area (shaded area). R: Rolling sphere Radius. H: Air termination rod length. P_L: Sphere penetration depth. d: Distance between two air termination rod.

Figure 4. Rolling sphere protection structure in PV system.

The same protection principle applies in a square-shaped system with four air termination rod at the same height at the corners. In the rolling sphere method, the penetration depth is calculated by Equation 48, [42].

$$P_L = \mathrm{R} - \sqrt{\mathrm{R}^2 - \left(\frac{\mathrm{d}}{2}\right)^2} \tag{48}$$

In PV systems, all the supporting metal parts in the area are connected to the 20x20 m strip conductor mesh grounding network [19]. Grounding the support structure and connecting it together with horizontal conductors act as an auxiliary electrode and potential equalization, reducing the cost, contact and step voltages [16],[44]. For the grounding facility discussed in this study, grounding calculations in accordance with the TT system were carried out. Equivalent diameter (D) is calculated by Equation 49 in earthing systems with mesh structure [31], [45].

$$D = \sqrt{\frac{4\ (ab)}{\pi}} \tag{49}$$

a and b are the width and length of the foundation grounding. Horizontal grounding resistance ($\mathrm{R_y}$) of horizontally laid mesh strip grounders is calculated according to Equation 50, and the approximate value of vertical grounding resistance ($\mathrm{R_d}$) of vertically buried rod and deep grounders is calculated by Equation 51 [37],[45]-[47].

$$\mathrm{R_y} = \frac{\rho_e}{2\mathrm{D}} + \frac{\rho_e}{\mathrm{L}} \tag{50}$$

$$\mathrm{R_d} = \frac{\rho_e}{\mathrm{nL}} \tag{51}$$

In the construction of a grounding system, different grounding systems are considered as parallel structures to each other and the equivalent grounding resistance ($\mathrm{R_e}$) is calculated by Equation 52 [31],[45].

$$\mathrm{R_e} = \frac{\mathrm{R_y\ R_d}}{\mathrm{R_y + R_d}} \tag{52}$$

The cross-section of the grounding conductor (A_{min}) must also be dimensioned with Equation 53 according to the thermal endurance caused by fault currents that can be interrupted within 5 s [46].

$$A_{min} = \frac{\mathrm{Ik_{1t}"}}{\mathrm{K}} \sqrt{\frac{\mathrm{t}}{\ln\frac{\theta_f + \beta}{\theta_i + \beta}}} \tag{53}$$

Where, $\mathrm{Ik_{1t}"}$ phase-ground short-circuit current, t fault current time, K is the conductor coefficient for the grounding conductor used (226 $\mathrm{A(s)^{1/2}/mm^2}$) for copper, β is the inverse of the temperature coefficient at zero C (234.5 °C for copper), θ_i is the initial temperature (20 °C), θ_f is the final temperature (300 °C) [46].

2.5 Optimum tilt angle calculation

Maximum solar radiation and maximum power generation are provided when sunlight comes to the solar panels with a vertical angle. However, this angle is constantly changing due to the earth's rotation around the tilted axis. In order to benefit from solar energy at the maximum level throughout the year, the tilt angle, which refers to the angle of the panel with the horizontal plane, should be adjusted to the most appropriate value. In this part of the study, the optimum tilt angle of the

panels for Denizli province was calculated with the method used in ref. [48]. Monthly average daily global solar radiation data (H) obtained from the Turkish Ministry of Energy and Natural Resources was used. The daily average extraterrestrial radiation H_0, is calculated by Equation 54.

$$H_0 = \frac{24}{\pi} I_{SC}\left(1 + 0.033\cos\frac{360n}{365}\right)\left(\cos\varphi\cos\delta\sin\omega_s + \frac{\pi\omega_s}{180}\sin\varphi\sin\delta\right) \quad (54)$$

Here I_{SC} is solar constant (=1353 W/m²), n is the day of the year, φ is the latitude, δ is the solar declination, ω_s is the hour angle. δ and ω_s are calculated by Equations 55 and 56.

$$\delta = 23.45\sin[360\ ((284 + n))/365] \quad (55)$$

$$\omega_s = \text{acos}(-\tan(\delta)\tan(\varphi)) \quad (56)$$

The average daily radiation (H_T) on an inclined surface can be calculated by Equation 57.

$$H_T = RH \quad (57)$$

Where R calculated by Equation 58 is the ratio of the average daily radiation on a sloped surface to that on a horizontal surface for each month.

$$R = \left(1 - \frac{H_d}{H}\right)R_b + H_d\left(\frac{1 + \cos(\beta)}{2H}\right) + \rho\left(\frac{1 - \cos(\beta)}{2}\right) \quad (58)$$

Where β is the solar panel tilt angle, ρ (=0.2) is the ground reflection. H_d, is the monthly average daily diffuse radiation and is calculated by Equation 59.

$$H_d = H(1.00 - 1.13K_T) \quad (59)$$

Here K_T is the monthly average clearness index and is given as in Equation 60.

$$K_T = {}^{H}/_{H_0} \quad (60)$$

R_b is the ratio of the average beam radiation on the tilted surface to that on the horizontal surface each month, calculated by the following Equation 61.

$$R_b = \frac{\cos(\varphi - \beta)\cos(\delta)\sin(\omega_s')}{\cos(\varphi)\cos(\delta)\sin(\omega_s) + \omega_s(\pi/180)\sin(\varphi)\sin(\delta)} + \frac{\omega_s'(\pi/180)\sin(\varphi - \beta)\sin(\delta)}{\cos(\varphi)\cos(\delta)\sin(\omega_s) + \omega_s(\pi/180)\sin(\varphi)\sin(\delta)} \quad (61)$$

Here, the sunset hour angle ω_s' for the tilted surface is calculated as Equation 62.

$$\omega_s' = \min\{\omega_s, \text{acos}[-\tan(\varphi - \beta)\tan(\delta)]\} \quad (62)$$

The monthly average daily total radiation on a south-facing surface was calculated by increasing the tilt angle from 0° to 90° in 1° steps. The optimum tilt angle was calculated by looking for the values at which the daily total solar radiation is maximum for a certain period of time.

3 Results and discussion

In the designed PV system, 400 kWe AC power generation is targeted. The power of each of the selected panels is 400 Wp. The panel/inverter ratio is assumed to be 1.351. Accordingly, the number of panels required was calculated as 1352. It should be taken into account that the panel can be connected in series up to the voltage value allowed by the inputs in string inverters. According to the panel inverter compatibility calculation, the maximum and minimum panel numbers that can be connected to the inverter inputs are calculated as $N_1 = 18.26, N_2 = 4.86$. Accordingly, it can be grouped as 60 string with 18 panels and 16 string with 17 panels. 4 inverters are required for the system. 15 strings with 18 solar panels and 4 strings with 17 panels are connected to each inverter inputs. Since the area covered by a panel is 2.048 m², a total of 2768.87 m² panel area and a total of 3626 m² roof area with security gaps are needed. The comparison of the values in Table 2 given in the inverter data sheet and the values calculated according to the panel-inverter compatibility calculation for the 18-panel string is given in Table 3.

Boztepe [49] emphasizes that in order to get maximum efficiency from a photovoltaic system, the panel and inverter must be compatible in terms of parameters such as maximum and minimum voltage and current value. Gazioğlu [50] states that the wide input operating voltage range in grid-connected solar inverters enables the inverter to start up earlier and turn off later in changing temperature/radiation conditions in the panels. According to Table 3 data, since the maximum and minimum open circuit voltages of the inverter are between the panel values, since the inverter MPPT values are between the panel MPPT values, the panel and the inverter are compatible with each other.

The results of current control, voltage drop and power loss calculations made to find the cable cross-sections of the DC and AC parts of the PV system are given in Table 4. While calculating the corrected current value for low voltage cables and busbars, the correction coefficients are taken from the manufacturers data [51],[52]. The busbar corrected current coefficients were calculated for 65 °C busbar temperature and 35 °C ambient temperature and vertical busbar. It is accepted that the cables are installed side by side in well-ventilated ducts at an ambient temperature of 35 °C at a conductor temperature of 70 °C.

Table 3. Panel inverter compatibility calculation values.

	$Voc_{max-dizi}$	$Voc_{min-dizi}$	$V_{MPPTmax-dizi}$	$V_{MPPTmin-dizi}$
Voltage (V)	985.61	781.72	827.30	656.18
Outcomes	$Voc_{max-dizi} < Vin_{max}$	$Voc_{min-dizi} > Vin_{min}$	$V_{MPPTmax-dizi} < V_{MPPTin-max}$	$V_{MPPTmin-dizi} > V_{MPPTin-min}$

Table 4. PV system current control, voltage drop and power loss calculation results.

Cable	Cross section (mm²)	Length (m)	Power (kW)	Cable (load) current (A)	Corrected current (A)	Voltage drop (e%)	Power loss (p%)
Cu_1	6	90	7.2	16.55	70	0.68	0.68
Cu_2	3x70+35	15	100	145	184	0.24	0.24
Cu_3	2(3x185+95)	25	400	578	669	0.60	0.60
Cu_4	4(4x1x95)	3	624	910 (max)	1086	0.22	0.22
Busbar	60x10	0.6	624	910 (max)	985	0.01	0.01

However, it should not be forgotten that the nominal current values of the breaker/thermal magnetic switch to be used in the facility must be greater than the cable corrected current values. According to the layout plan, DC voltage drop calculation was made for the longest string. As stated byAydöner [53] and Öncin [54] the solar cable maximum current was calculated by multiplying the panel short-circuit current by 1.25 twice, based on over-radiation and safety factor.

According to Ekici ve Kopru [11] in many well-designed PV systems, DC cable losses should be less than 2% and voltage drop should be less than 1.5%. In AC system, the voltage drop should be less than 3%. Since the percentage of voltage drop and the percentage of power loss for the selected sections are smaller than the critical values and the cable corrected current carrying capacity is larger than the load current, it can be seen from Table 4 that the sections are suitable. When the voltage drop and power loss are calculated according to a lower cross section in the plant sections, the voltage drop and power loss are smaller than the critical value, but the load current is greater than the cable current carrying capacity. The reason why the percentage of voltage drop for the facility is very small is due to the short cable lengths. Accordingly, it can be said that the cable sections in the system are selected according to the current carrying capacity.

If a copper busbar is used in the PV panel in the facility, its cross-section should be at least 60x5 mm^2 in terms of current carrying capacity according to the maximum power of the PV system. The positive, negative and zero sequence component pu resistance and reactance values of the grid connection sections used in short circuit calculations in the system were calculated as in Table 5.

The results of the short circuit calculations made for the A (transformer HV busbar) and B (transformer LV busbar) points of the system are given in Table 6.

According to Table 6, the highest short-circuit current at point A is three-phase short-circuit current, and at point B, two-phase ground short-circuit current. For the thermal short-circuit current calculation, the k value is 1.5 at A point, 1.97 at B point, m value is 0.0294 at A point and 0.8289 at B point. Current transformers are selected by using the upper standard value of the coefficient obtained according to the thermal short circuit current (I_{th}) value passing through the line to which it is connected. Büyükdora [55], Karaca [56], Kaşıkçı [57] indicate that the primary thermal withstand current value can be 40, 100, 200, ...1200 times the primary rated current. Büyükdora [55], İnan et al. [30] explain that current transformers should be able to withstand the thermal and dynamic effects of short-circuit currents, and the dynamic effect can be around 2.5 times the thermal effect.

İriz [32] emphasizes that the thermal withstand current of the current transformer, which is the primary current value that it can withstand without being damaged for 1 s when the secondary is short-circuited, causes an increase in cost when I_{thCT} is greater than necessary. In the selection of the breaker, it should also be noted that the closing capacity is greater than the peak short-circuit current current according to IEC60947.

As stated by İnan et al. [30] and Kaşıkçı [57] the breaking power of the breakers was calculated by taking 1.1 times the three-phase short-circuit current for point A and 1.25 times the two-phase earth short-circuit current for point B.

The conductor cross-sections of the A and B sections of the transformer were also calculated according to the thermal short circuit current. The bending stress value of the low voltage busbars were calculated according to the peak short circuit current. The calculated values (CV) and the selected/standard values (SV) are given in Table 7.

An upper standard cross section is selected according to the thermal short circuit current value calculated on the high voltage side of the TS 2 transformer. Although the low voltage side cable and busbar cross-sections were smaller than the thermal short-circuit current, larger cross sections are required due to current control calculation results. While the distance between the 80 cm long copper busbars placed vertically on the support insulators on the low voltage side is 10 cm, the bending stress is calculated to be less than the critical value. Data in Kasikci [36] and Panelmaster [51] were taken as the critical value. Kasikci [36] and Szulborski et al. [35] state that the calculated bending stress value should be less than the critical value so that the busbars do not deform in possible peak short-circuit current.

In the grid-connected PV system, the facility edge length values are calculated as approximately 74 and 49 m, according to the panel positions. The grounding resistance values calculated for the facilitys foundation grounding network and the minimum grounding conductor cross-section calculated according to the short-circuit current are given in Table 8.

As indicated by the critical resistance Megep [45] in the basic grounding, it was calculated and compared for the 300 mA residual current protection trip current value under 50V voltage. The grounding resistance of the facility was found to be less than the critical value (0.86<166.67). As can be seen in Table 8, the minimum grounding conductor cross-section is calculated as 53.97 mm^2 copper conductor according to the thermal resistance based on the low voltage side phase ground short circuit current.

The lightning risk calculation was made with the assumptions that the facility is higher than the surrounding buildings, the roof is aluminum sandwich panel, the walls are brick-concrete, the building is non-flammable, normally crowded, in continuous use and in continuous use. According to the results given in Table 9, protection is required in the PV system since Nc<Nd.

According to the calculated protection efficiency value, the protection level was determined as the fourth level. According to the calculated E value, as stated in Ürgüplü [40] IV. level of protection is required. At this level, the sphere radius should be taken as 60 m. The penetration depth of the sphere was calculated as 0.84 m, since it is assumed that the air terminetion rods are placed at 20 m intervals in the facility. In this case, for the panel to be within the protection zone, the height of the air termination rods must be higher than 0.84 m from the highest point of the panel.

In order to benefit from the solar radiation at maximum level in Denizli, the monthly, seasonal and annual optimum values of the tilt angle are given in the Figure 5.

Table 5. Sequence component values (pu) according to 100MVA base apparent power.

Sections	PS, NS (R1, R2)	PS, NS (X1, X2)	ZS (R0)	ZS (R0)	ZS (X0)
Transmission Network	0.010	0.099	0.010	0.010	0.197
TS 1		0.137			0.137
Neutral resistance			18.141	18.141	
H1	0.002	0.002	0.012	0.012	0.006
H2	0.017	0.019	0.025	0.025	0.058
H3	0.041	0.047	0.059	0.059	0.140
H4	0.002	0.001	0.006	0.006	0.004
TS 2		9.524			9.524
Total	0.071	9.828	18.252	18.252	10.067

Table 6. Short circuit calculation results.

	$Ik_3^{"}$ (kA)	Ik_2" (kA)	Ik_{1t}" (kA)	Ik_{2t}" (kA)	I_p (kA)	I_{th} (kA)	I_{thCT} (A)	Sa" (MVA)
A bus	5.88	5.09	0.29	0.15	12.52	4.22	365.03 I_n	352.47
B bus	14.70	12.73	14.86	15.01	42.02	14.36	15.78 I_n	12.99

Table 7. Conductor cross section and bending stress.

	$q_{thA}(mm^2)$	$q_{thB}(mm^2)$	$q_{thbara}(mm^2)$	$\sigma_g(kN/cm^2)$
CV	44.87	124.87	119.67	28.25
SV	50.00	380.00	600.00	30.00

Table 8. Calculation results related to grounding.

D (m)	R_y (Ω)	R_d(Ω)	R_e(Ω)	A_{min} (mm^2)
67.96	1.14	3.57	0.86	53.97

Table 9. Lightning protection system calculation results.

H (m)	$A_e(m^2)$	N_g	N_d	N_c	E	P_L (m)
9	12558.22	0.8934	0.0056	0.0022	0.61	0.84

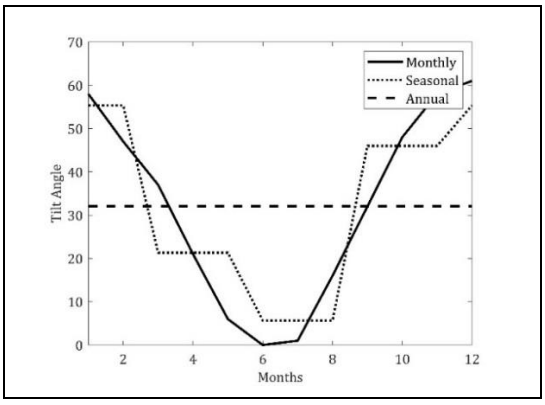

Figure 5. Monthly, seasonal and annual (fixed) optimum tilt angles.

The Figure 5 shows that the optimum tilt angle varies between 0° (June) and 61° (December) throughout the year. The seasonal variation is between 5.67° (summer) and 55.33° (winter). The fixed optimum tilt angle is 32.08°. Tilt angle change is same the literatüre [59]-[62].

4 Conclusions

In this study, the electrical calculations required for the selection of 0.4 MWe grid-connected PV system operation and protection equipment are presented. In this context, first of all, panel-inverter compatibility calculations were made and then current control and voltage drop calculations were made to determine the low voltage conductor cross-sections. Short-circuit calculations were made for the selection of line sections, current transformers, breakers and the determination of the bending stress in the low voltage busbars in the integration line to the grid. In addition, lightning risk calculation for the facility, protection area calculation according to the rolling sphere method, network grounding resistance calculation and minimum grounding conductor cross-section calculation according to the short circuit current were made.

The number of panels being more than the calculated value causes the inverter allowable input voltage range to be exceeded, while it is less causes the decrease maximum power generation of the inverter. In the selection of the cables used to carry the power produced from the solar panels to the solar energy board, the current carrying capacity of the cables in short distances had a greater effect, while the effect of voltage drop increased at longer distances. If the cross-section is smaller than the calculated value, it causes the cable to be overloaded and the voltage drop in the cable to be increase higher values. On the other hand, if the cross-section is much higher than the calculated value, it will cause an unnecessary increase in the cost. Turkey uses 36.52% of its electricity generation potential based on renewable energy. Between 2021-2024, the amount of carbon dioxide emission reduction that can be achieved by electricity generation from renewable energy sources is expected to be approximately 455 metric tons of carbon dioxide equivalent. In Turkey, which has a high solar energy potential, the rate of solar energy utilization is still 13.9% [58]. Increasing the rate of utilization of solar energy is of great importance. The calculations made in this study enable the selection of appropriate protection and operating equipment for PV systems. Appropriate equipment in PV systems will reduce installation and operating costs and make a significant contribution to the widespread use of the system.

5 Author contribution statements

Ahmet ILICA idea formed, designed the article, conducted the literature review, performed analyzes, discussed the results and wrote the article. Muhammed SERDAR collected the data, checked the article in terms of content.

6 Ethics committee approval and conflict of interest statement

"There is no need to obtain permission from the ethics ommittee for the article prepared".

"There is no conflict of interest with any person/institution in the article prepared".

7 References

[1] Islam S, Woyte A, Belmans R, Nijs J. "Undersizing inverters for grid connection-what is the optimum?". *Proceedings of the 18th Symposium Photovoltaic Solar-Energy*, Bad Staffelstein, Germany, 12-14 March 2003.

[2] Rauf A, Al-Awami AT, Kassas M, Khalid M. "Optimal sizing and cost minimization of solar photovoltaic power system considering economical perspectives and net metering schemes". *Electronics,* 10(21), 1-18, 2021.

[3] Ürün E, Soyu E. "Türkiye'nin enerji üretiminde yenilenebilir enerji kaynakları üzerine bir değerlendirme". *Dumlupınar Üniversitesi Sosyal Bilimler Dergisi*, ICEBSS Özel Sayısı, 31-45, 2016.

[4] Luque A. "Photovoltaic market and costs forecast based on a demand elasticity model". *Progress in Photovoltaics: Research and Applications*, 9(4), 303-312, 2001.

[5] Moussa I, Khedher A, Bouallegue A. "Design of a low-cost PV emulator applied for PVECS". *Electronics*, 8(2), 1-15, 2019.

[6] Arici N, İskender A. "Fotovoltaik güneş santrallerinde şebeke bağlantı sorunları ve çözümleri". *Politeknik Dergisi*, 23(1), 215-222, 2020.

[7] Malamaki KD, Demoulias CS, Member S. "Analytical calculation of the electrical energy losses on fixed-mounted PV plants". *IEEE Transactions on Sustainable Energy*, 5(4), 1080-1089, 2014.

[8] Bayram M. Fotovoltaik Güç Sistemlerinde Maksimum Güç Noktasının Gerçek Zamanlı Olarak Izlenmesi. Yüksek Lisans Tezi, Bursa Teknik Üniversitesi, Bursa, Türkiye, 2019.

[9] Duman S. Şebeke Bağlantısız Güneş ve Rüzgar Enerji Sistemlerinin Yönetimi, Kontrolü ve Izlenmesi için Yeni Yaklaşımlar. Doktora Tezi, Kocaeli Üniversitesi, Kocaeli, Türkiye, 2015.

[10] Cramer G, Ibrahim M, Kleinkauf W. "PV system technologies-state of the art and trends in decentralised electrification". *Refocus*, 5(1), 38-42, 2004.

[11] Ekici S, Kopru MA. "Investigation of PV system cable losses". *International Journal of Renewable Energy Research*, 7(2), 807-815, 2017.

[12] Mosheer AD, Gan CK. "Optimal solar cable selection for photovoltaic systems". *Journal of Renewable Energy Resources*, 5(2), 28-37, 2015.

[13] Kaşıkçı İ. *Elektrik Mühendisliği Elektrik Enerjisinin Üretimi İletimi Dağıtımı*. 1. Baskı. İstanbul, Türkiye, Birsen, 2013.

[14] Datsios ZG, Mikropoulos PN. "Safe grounding system design for a photovoltaic power station". *In 8th Mediterranean Conference on Power Generation, Transmission, Distribution and Energy Conversion*, Cagliari, Italy, 1-3 October 2012.

[15] Nassereddine M, Ali K, Nohra C. "Photovoltaic solar farm: earthing system design for cost reduction and system compliance". *International Journal of Electrical and Computer Engineering*, 10(3), 2884-2893, 2020.

[16] Zhang Y, Li B, Du Y, Ding Y, Cao J, Lv J. "Effective grounding of the photovoltaic power plant protected by lightning rods". *IEEE Transactions on Electromagnetic Compatibility*, 63(4), 1128-1136, 2021.

[17] Damianaki K, Christodoulou CA, Kokalis CA, Kyritsis A, Ellinas ED, Vita V, Gonos, IF. "Lightning protection of photovoltaic systems: computation of the developed potentials". *Applied Sciences*, 11(1), 1-12, 2021.

[18] Kalenderli Ö. "Yıldırımdan korunma". *EMO İzmir Şubesi Haber Bülteni*, 249, 14-16, 2011.

[19] Charalambous CA, Kokkinos ND, Christofides N. "External lightning protection and grounding in large-scale photovoltaic applications". *IEEE Transactions on Electromagnetic Compatibility*, 56(2), 427-434, 2013.

[20] Kareem MSA, Saravanan M. "A new method for accurate estimation of PV module parameters and extraction of maximum power point under varying environmental conditions". *Turkish Journal of Electrical Engineering and Computer Sciences*, 24(4), 2028-2041, 2016.

[21] Setiawan EA, Setiawan A, Siregar D. "Analysis on solar panel performance and pv-inverter configuration for tropical region". *Journal of Thermal Engineering*, 3(3), 1259-1270, 2017.

[22] Güven Ş. "Investigation of the effect of photovoltaic panel surface temperature on output power and efficıency in Denizli". *Engineer and Machinery*, 63(707), 429-442, 2022.

[23] Luoma J, Kleissl J, Murray K. "Optimal inverter sizing considering cloud enhancement". *Solar Energy*, 86(1), 421-429, 2012.

[24] Ramli MAM, Hiendro A, Sedraoui K, Twaha S. "Optimal sizing of grid-connected photovoltaic energy system in Saudi Arabia". *Renewable Energy*, 75, 489-495, 2015.

[25] Kil AJ, Van der Weiden TCJ. "Performance of modular grid connected PV systems with undersized inverters in Portugal and the Netherlands". *IEEE 1st World Conference on Photovoltaic Energy Conversion*, Hawaii, USA, 05-09 December 1994.

[26] Burger B, Rüther R. "Inverter sizing of grid-connected photovoltaic systems in the light of local solar resource distribution characteristics and temperature". *Solar Energy*, 80(1), 32-45, 2006.

[27] Mondol JD, Yohanis YG, Norton B. "Optimal sizing of array and inverter for grid-connected photovoltaic systems". *Solar Energy*, 80(12), 1517-1539, 2006.

[28] Macêdo WN, Zilles R. "Operational results of grid-connected photovoltaic system with different inverter's sizing factors (ISF)". *Progress in Photovoltaics: Research and Applications*, 15(4), 337-352, 2007.

[29] Liu Y, Yu R, Zhang L, Jiang D, Chen N, Zhao D. "Research on short-circuit currents calculation method considering dynamic reactive power support of renewable energy systems". *2nd IEEE Conference on Energy Internet and Energy System Integration*, Beijing, China 20-22 October 2018.

[30] İnan A, Tercan SM, Kara H. *Orta Gerilim Transformatör Merkezlerinin Projelendirilmesi*. 1. Baskı. İstanbul, Türkiye, Birsen, 2012.
[31] Yücel ME. *Endüstriyel Elektrik*. 1. Baskı. Ankara, Türkiye, Grafiker, 2002.
[32] İriz T. "Akım transformatörlerinde kısa süreli termik anma akımının hesaplanması". *EMO İzmir Şubesi Haber Bülteni*, 209, 11-12, 2007.
[33] Kaşıkçı İ. *Elektrik Tesisleri Temel El Kitabı*. 1. Baskı. Istanbul, Türkiye, Birsen, 2008.
[34] Pamuk N. "Sakarya ili Sapanca ilçesinin Adapazarı ve Kırkpınar trafo merkezlerinden beslenmesi durumundaki kısa devre güçlerinin karşılaştırılması ve uygun koruma elemanlarının belirlenmesi". *Erciyes Üniversitesi Fen Bilimleri Dergisi*, 27(1), 48-61, 2011.
[35] Szulborski M, Lapczynski S, Kolimas L, Kozarek L, Rasolomampionona DD. "Calculations of electrodynamic forces in three-phase asymmetric busbar system with the use of FEM". *Energies*, 13(20), 1-26, 2020.
[36] Kasikci I. *Short Circuits in Power Systems: A Practical Guide to IEC 60909-0*. 2nd Ed. Wiley, 2018.
[37] Kaşıkçı İ. *Elektrik Tesisleri Güvenlik Koruma ve Uygulama Esasları*. 1. Baskı. İstanbul, Türkiye, Birsen, 2018.
[38] Furse. "A Guide to BS EN 62305 Protection Against Lightning". https://www.jac.ie/wp-content/upload/pdf/Guide to BS 62305 3rd edition.pdf (19. 04. 2022).
[39] Orak V. İstanbul Üniversitesi Avcılar Yerleşkesi Yıldırım Risk Analizi. Yüksek Lisans Tezi, İstanbul Üniversitesi, İstanbul, Türkiye, 2018.
[40] Ürgüplü Z. *Elektrobank, Elektroteknik Bilgi Bankası*. 2. Baskı. Ankara, Türkiye, Bizim Büro, 2008.
[41] Ayub AS, Siew WH, Mohamed FP. "Grounding strategies for solar PV panels". *IEEE Asia-Pacific Symposium on Electromagnetic Compatibility*. Suntec City, Singapore, 14-18 May 2018.
[42] Kalenderli Ö. "Yıldırımdan Korunma". https://www.yilkomer.com/wpcontent/uploads/2016/02/yildırımdan korunma-standartı.pdf (20. 04. 2022).
[43] Stefanescu S, Botezan A. "Overview of the protection lightning standards suite EN/IEC 62305". *International Conference and Exposition on Electrical and Power Engineering*, Iasi, Romania, 20-22 October 2016.
[44] Schaerer R, Lewis D. "Large utility-scale photovoltaic solar power plant grounding system safety design-general practices and guidance". *IEEE Power & Energy Society General Meeting*, Denver, USA 26-30 July 2015.
[45] Megep. "Topraklama projeleri". https://megep.meb.gov.tr/mte_program_modul/moduller_pdf/Topraklama%20Projeleri.pdf (15.03.2022).
[46] MENR. "Elektrik tesislerinde topraklamalar yönetmeliği". https://www.mevzuat.gov.tr/mevzuat?MevzuatNo=10392&MevzuatTur=7&MevzuatTertip=5 (03.06.2022).
[47] Kaşıkçı İ. *AG Elektrik Tesislerinde Topraklama ve Ölçme*. 1. Baskı. İstanbul, Türkiye, Birsen, 2010.
[48] Bakirci K. "General models for optimum tilt angles of solar panels: Turkey case study". *Renewable and Sustainable Energy Reviews*, 16(8), 6149-6159, 2012.
[49] Boztepe M. İzmir (Bornova) Koşullarında Şebekeye Bağlı Fotovoltaik Bir Sistemin Tasarlanıp Denenmesi. Doktora Tezi, Ege Üniversitesi, İzmir, Türkiye, 2002.
[50] Gazioğlu Ç. "Güneş enerji sistemlerinde solar invertör seçimi(EMO Ankara Şubesi webinar)". https://www.youtube.com/watch?v=EfBxIZLut4s (15. 10. 2022).
[51] Panelmaster. "B Serisi Bakır Bara Düzenekleri Uygulama Kılavuzu". https://tw.eae-et.com.tr/TW/ MDokDb.nsf/xvDokTur.xsp?categoryFilter=Katalog%5CPanelMaster%5CT%C3%BCm%20%C3%9Cr%C3%BCn%20Gruplar%C4%B1 (10. 06. 2022).
[52] Heskablo. "Enerji kabloları ürün kataloğu". https://www.hes.com.tr/urun-kataloglari (10.05. 2022).
[53] Aydöner D. Binaya Entegre Fotovoltaik Sistem Tasarımı ve Kurulumu. Yüksek Lisans Tezi, Gebze Yüksek Teknoloji Enstitüsü, Kocaeli, Türkiye, 2010.
[54] Öncin F. Çatı Tipi Güneş Enerji Santralleri ve Dağıtım Tesislerine Bağlantı Kriterleri. Yüksek Lisans Tezi, Gazi Üniversitesi, Ankara, Türkiye, 2018.
[55] Büyükdora H. "Ölçü Trafoları". https://www.emo.org.tr/ekler/90efb66c5016fa8_ek.pdf (25.07.2022).
[56] Karaca S. "Akım Trafosu". https://elektroloji.com/koruma-sistemleri/akim-trafosu.html (16. 03. 2022).
[57] Kaşıkçı I. *Elektrik Tesislerinde Kısa Devre Hesapları ve Uygulamaları*. 1. Baskı. İstanbul, Türkiye, Birsen, 2007.
[58] Ozcan M. "Increasing voluntary carbon credits potential via renewable energy projects in Turkey". *Pamukkale Üniversitesi Mühendislik Bilimleri Dergisi*, 28(5), 710-719, 2022.
[59] Karafil A, Ozbay H, Kesler M, Parmaksiz H. "Calculation of optimum fixed tilt angle of PV panels depending on solar angles and comparison of the results with experimental study conducted in summer in Bilecik, Turkey". *In 2015 9th International Conference on Electrical and Electronics Engineering*, Bursa, Turkey 26-28 November 2015.
[60] Buzra U, Mitrushi D, Serdari E, Halili D, Muda V. "Fixed and adjusted optimal tilt angle of solar panels in three cities in Albania". *Journal of Energy Systems*, 6(2), 153-164, 2022.
[61] Arslan M, Cunkas M. "A Study on Optimum Tilt Angle of PV Panels for Konya, Turkey". *57th International Scientific Conference on Information, Communication and Energy Systems and Technologies*, Ohrid, North Macedonia, 16-18 June 2022.
[62] Sumair M, Aized T, Mahmood M, Bhutta A, Shoaib M. "Computing optimum solar tilt angles for photovoltaic applications through python code simulation". *Environmental Progress & Sustainable Energy*, 42(5), 1-15, 2023.